ANTICANCER RESEARCH *37*: 1139-1148 (2017)
doi:10.21873/anticanres.11427

# Relationship Between $K_{trans}$ and $K_1$ with Simultaneous *Versus* Separate MR/PET in Rabbits with VX2 Tumors

KYUNG HEE LEE[1,2*], SEUNG KWAN KANG[3,4*], JIN MO GOO[1,5,6], JAE SUNG LEE[3,4], GI JEONG CHEON[3,5], SEONGHO SEO[7] and EUI JIN HWANG[1,8]

[1]*Department of Radiology, Seoul National University Hospital, Seoul National University College of Medicine, Seoul, Republic of Korea;*
[2]*Department of Radiology, Seoul National University Bundang Hospital, Seongnam, Republic of Korea;*
[3]*Department of Nuclear Medicine, Seoul National University Hospital, Seoul National University College of Medicine, Seoul, Republic of Korea;*
[4]*Department of Biomedical Sciences, Seoul National University College of Medicine, Seoul, Republic of Korea;*
[5]*Institute of Radiation Medicine, Seoul National University Medical Research Center, Seoul, Republic of Korea;*
[6]*Cancer Research Institute, Seoul National University College of Medicine, Seoul, Republic of Korea;*
[7]*Department of Neuroscience, College of Medicine, Gachon University, Incheon, Republic of Korea;*
[8]*Armed Forces Seoul Hospital, Seoul, Republic of Korea*

**Abstract.** *Background/Aim: To compare the relationship between $K_{trans}$ from DCE-MRI and $K_1$ from dynamic $^{13}$N-$NH_3$-PET, with simultaneous and separate MR/PET in the VX-2 rabbit carcinoma model. Materials and Methods: MR/PET was performed simultaneously and separately, 14 and 15 days after VX-2 tumor implantation at the paravertebral muscle. The $K_{trans}$ and $K_1$ values were estimated using an in-house software program. The relationships between $K_{trans}$ and $K_1$ were analyzed using Pearson's correlation coefficients and linear/non-linear regression function. Results: Assuming a linear relationship, $K_{trans}$ and $K_1$ exhibited a moderate positive correlations with both simultaneous (r=0.54-0.57) and separate (r=0.53-0.69) imaging. However, while the $K_{trans}$ and $K_1$ from separate imaging were linearly correlated, those from simultaneous imaging exhibited a non-linear relationship. The amount of change in $K_1$ associated with a unit increase in $K_{trans}$ varied depending on $K_{trans}$ values. Conclusion: The relationship between $K_{trans}$ and $K_1$ may be mis-interpreted with separate MR and PET acquisition.*

Dynamic contrast-enhanced magnetic resonance imaging (DCE-MRI) parameters are widely used for assessment of treatment response to anti-angiogenic drugs in both preclinical studies and clinical trials (1, 2). The main advantages of DCE-MRI are its high spatial resolution and nonuse of ionizing radiation (3, 4). However, absolute quantification of flow is difficult and interpretation of DCE-MRI data is complicated. Dynamic $^{13}$N-$NH_3$ positron emission tomography (PET) primarily reflects blood flow because NH3 has a high extraction fraction; therefore, interpretation $^{13}$N-$NH_3$ PET parameters is more straightforward (5, 6). While dynamic $^{13}$N-$NH_3$ PET has been clinically utilized in myocardial perfusion imaging (5, 6), its utility in tumor imaging is under-investigated. However, several reports involving this technique have demonstrated promising results in the diagnosis of brain tumors and fibrosarcomas (7-10). Knowledge of the quantitative perfusion parameters of dynamic $^{13}$N-$NH_3$ PET and the relationship between MR and PET parameters might enhance our understanding of angiogenesis and vascular permeability (11).

With the recently introduced hybrid MR/PET, DCE-MRI and dynamic $^{13}$N-$NH_3$ PET images can be obtained simultaneously with perfect temporal and much improved

*These Authors contributed equally to this study.

*Correspondence to:* Jin Mo Goo, M.D., Department of Radiology, Seoul National University College of Medicine, and the Institute of Radiation Medicine, Seoul National University Medical Research Center, 101 Daehak-ro, Jongno-gu, Seoul 110-744, Republic of Korea. Tel: +82 220722624, Fax: +82 27437418, e-mail: jmgoo@plaza.snu.ac.kr and Jae Sung Lee, Ph.D., Department of Nuclear Medicine, Seoul National University College of Medicine, 101 Daehak-ro, Jongno-gu, Seoul 110-744, Republic of Korea. Tel: +82 220722938, Fax: +82 27452938, e-mail: jaes@snu.ac.kr

*Key Words:* MR/PET, dynamic contrast enhanced-MRI, $^{13}$N-$NH_3$ PET, perfusion parameter, rabbit.

spatial co-registration (12-14). The simultaneity of hybrid MR/PET systems offers several advantages over separate MR and PET and PET/computed tomography (15, 16), including precise patient alignment, recording of dynamic phenomena, tissue information under identical physiologic state from both modalities, and better localization of PET signals in soft tissues (17). In terms of patient alignment, a previous study reported better alignment quality with simultaneous MR/PET than with retrospective fusion of MR and PET data (18). However, there is a paucity of studies evaluating the simultaneity of hybrid MR/PET systems based on functional information and verifying its clinical implications. The purpose of this study was to compare the relationship between $K_{trans}$ from DCE-MRI and $K_1$ from dynamic $^{13}N$-$NH_3$-PET, with simultaneous and separate MR/PET in the VX-2 rabbit carcinoma model.

## Materials and Methods

*Animal model*. This study was approved by the Animal Care and Use Committee in our institution (Permit number: 13-0394-C1A1(3)). Eight adult New Zealand white rabbits weighing 3.0-3.5 kg, were included in this study. The rabbit VX2 tumor model was chosen for the following reasons; (i) it is a reliable transplantable tumor model that has not been well established in large animals (19), (ii) rodents are too small in size to obtain reliable perfusion parameters with MR/PET; (iii) many previous studies have employed the rabbit VX2 tumor model for DCE-MR imaging (20, 21) and the preclinical animal experimental center of our institute periodically inoculates VX2 cells into the thigh muscles of New Zealand White rabbits to maintain *in vivo* passages of VX2 cells, thus making the cells easily accessible for this study.

Prior to tumor implantation, animals were sedated by intravenous injection of 5 mg/kg of a 1:1 combination of tiletamine hydrochloride and zolazepam (Zoletil; Virbac, Carros, France) and xylazine hydrochloride (Rompun 2%; Bayer Korea, Seoul, Korea). After anesthesia and shaving of the paravertebral area, 0.2 ml of a suspension of finely minced fresh VX2 tumor was implanted in the left paravertebral muscle at the level of heart, using 16-gauge Medicut needles under ultrasonographic guidance. The heart was required to be within the scan range in order to measure the arterial input function of dynamic PET. Two weeks after tumor implantation, the VX2 tumors were expected to be approximately 2 cm along the longest dimension, appropriate for tumor perfusion imaging. Each rabbit was subjected to MR/PET (Biograph mMR, Siemens Healthcare, Erlangen, Germany) on two successive days 14 days after tumor implantation. All efforts were made to minimize the suffering of animals during tumor implantation and MR/PET.

*MR/PET*. Rabbits were anesthetized, and a 20-gauge intra-venous cannula (Medicut) was inserted into the right marginal ear vein before the start of MR/PET. The MR/PET acquisition protocol is illustrated in Figure 1. Simultaneous MR and PET image acquisition was performed 14 days after tumor implantation. For dynamic MR/PET, 0.2 mmol/kg gadoterate meglumine (Dotarem; Guerbet, Bloomington, IN, USA) and 111 MBq $^{13}N$-$NH_3$ were hand injected simultaneously using three-way stopcocks, followed by 8 ml saline chaser. Since we planned on examining two rabbits per synthesis of $^{13}N$-$NH_3$ (up to 200mCi/cassette), the total injection volume of MR and PET contrast media was made up to 2 ml by dilution with normal saline to maintain uniform concentration of MR contrast media at every examination. Contrast media was injected slowly over a 30-s duration. The total scan time was approximately 25 min. Separate MRI and PET image acquisition was performed 15 days after tumor implantation. After completion of PET, the rabbits were removed from the MR/PET scanner and placed back inside the scanner approximately 60 minutes later. The animals were positioned on their back at the same level as the MRI table. The injection dose, volume and method of MR and PET contrast media were maintained the same between simultaneous and separate imaging. However, during separate MR and PET, 2 ml normal saline was hand injected simultaneously as the control. The total examination time for separate imaging was approximately 40 min. Scanning parameters for PET and MRI were maintained the same for simultaneous and separate imaging, as described below.

*DCE-MRI parameters*. All MR images were acquired using dedicated head and body coils approved for MR/PET at the same time. T2-weighted imaging (T2WI) was performed with the following parameters: repetition time/echo time (TR/TE), 4100/87 ms; matrix size, 128×128; slice thickness, 3 mm; and field of view (FOV), 130×130 mm. Pre-T1-weighted (T1W) images were acquired with a gradient echo sequence (weighted volumetric interpolated breath-hold examination [VIBE]) at each of the four flip angles for T1 mapping using the following parameters: TR/TE 4.4/1.1 ms; flip angles ($\alpha$=2°, 5°, 10° and 15°); matrix size 128×128; slice thickness 3 mm; number of slices 20; and 130×130 mm. Using the VIBE sequence, DCE-MR images were obtained at 5 s of temporal resolution with the following parameters: TR/TE, 3.5/1.5 ms; flip angles ($\alpha$=11°); matrix size 128×128; slice thickness, 3 mm; number of slices, 20; and FOV, 130×130 mm. The total acquisition time of dynamic scan including the first six phases of pre-contrast images was 10 min.

*Dynamic $^{13}N$-$NH_3$ PET parameters*. An approximately 20-s T1W Dixon gradient-echo sequence image in the coronal plane was first acquired for attenuation correction. Then, the emission protocol of a 10-min dynamic scan (6×5 s [precontrast]); 12×5 s; 3×10 s; 6×30 s; 2×60 s; and 1×180 s) was implemented. The 30-s precontrast phase was included to maintain uniformity between dynamic $^{13}N$-$NH_3$ PET and DCE-MRI. Dynamic PET images were reconstructed by point spread function modeling.

*Image analysis*. One board, certified radiologist (K.H.L.), with four years of experience after board certification) measured the long and short diameters of tumors on axial T2WI. In addition, the same radiologist manually drew region-of-interests (ROIs) on the left ventricle and tumors on DCE-MR images using MRIcro (http://www.sph.sc.edu/comd/rorden/mricro.html). To derive individual arterial input function (AIF) curves, ROIs were drawn in the left ventricle in three or four different image slices in the peak arterial enhancement phase of imaging. The radiologist also manually drew ROIs on tumors by outlining the entire tumor boundary as delineated by contrast enhancement in all involved MR slices containing the tumor.

*In-house software program development*. We developed an in-house software program using customized matrix laboratory (MATLAB) scripts (The Mathworks Inc., Natick, MA, USA) to generate $K_{trans}$ and K1 maps on ROI- and voxel-level from DCE-MRI and $^{13}N$-

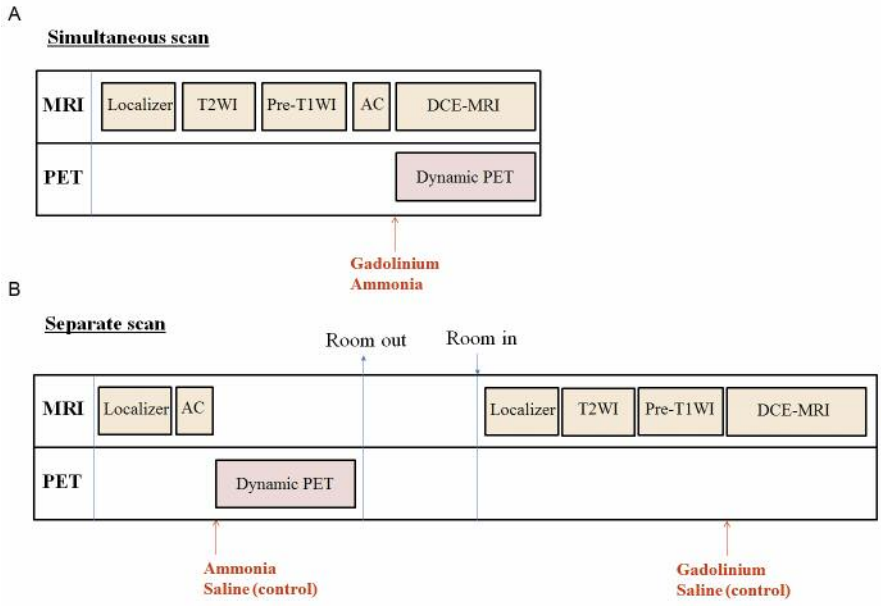


Figure 1. *Schematic drawing of the MR/PET acquisition protocol. (A) Simultaneous MR/PET acquisition and (B) Separate MR and PET acquisition 14 and 15 days after tumor implantation, respectively.*

$NH_3$ PET using individual AIF curves. For simultaneous image acquisition, the MR and PET data were resampled to match the image coordinates and dimensions. For separately acquired MR and PET images, registration was processed using SPM software (Statistical Parametric Mapping, SPM12). The details of the in-house software program are described below.

*Tumor perfusion parameters from DCE-MRI*. i) Pre-processing of T1 signals in DCE-MRI: Baseline T1 signal was measured using pre-T1 images acquired at four different flip angles. Three-dimensional (3D) $R1_0$ and $S_0$ maps were calculated based on the Ernst formula (TE << T2*) using four sets of gradient recalled echo (GRE) images with different flip angles. A linear least square method was used for calculation of the 3D $R1_0$ and $S_0$ maps (22). ii) Estimation of contrast agent concentration time curves: Four-dimensional (4D; x, y, z, t) post-injection longitudinal relaxation rate (R1(t)) maps were calculated for each dynamic phase using signal intensity data from the pre- and post-contrast T1W-GRE dynamic series:

$$R1(t) = -(1/TR)\times \ln\frac{1-(A+B)}{1-\cos\theta\times(A+B)}$$

where α=11˚; TR=3.5 seconds;

$$A=\frac{S(t)-S(0)}{S_0\sin\theta};\quad B=\frac{1-E_{10}}{1-\cos\theta\cdot E_{10}};\quad E_{10}=\exp(-TR\times R_{10});$$

and S(0) and S(t) are the signal intensities of images in the 4D T1W-GRE dynamic series before and after contrast injection. 4D gadoterate meglumine concentration maps (x, y, z, t) in tissues [$C_t(t)$] were calculated from 4D $R_1(t)$ maps as follows: $R_1(t)=R_{10}+r_1 x C_t(t)$, where $r_1$ is the experimentally determined relaxivity of gadoterate meglumine and $r^1$=4.5 $mM^{-1}s^{-1}$ (at 37˚). iii) Determination of individual AIF: For each patient, concentration maps in blood ($C_b(t)$ maps) were calculated based on the ROI in the left ventricle. Concentration maps in the plasma ($C_p(t)$ maps) were calculated from $C_b(t)$ maps using the following equation, where hematocrit (Hct) was 0.4:

$$C_p(t)=\frac{C_b(t)}{1-Hct}.$$

iv) Parameter estimation for a given compartmental model: 3D perfusion parameter ($K_{trans}$) maps were calculated from the $C_p(t)$ and 4D C(t) maps using the single-tissue compartment modified Tofts model:

$$C_t(t)=K_{trans}\int_0^t C_p(u)\cdot e^{-(K_{trans}/V_e)(t-u)}du+v_pC_p(t).$$

*Tumor perfusion parameters from $^{13}N$-$NH_3$ PET*. Perfusion parameters from $^{13}N$-$NH_3$ PET were calculated using several different methods. First, they were quantified using a 2-tissue (2TCM) or 1-tissue (1TCM) compartment model. Goodness-of-fit factors (the Akaike information [AIC], Schwartz [SC], and model selection [MSC] criteria) were calculated for comparison of 1TCM and 2TCM perfusion parameters. Second, at the ROI-level, perfusion parameters were estimated from a single time-activity curve (TAC) of ROI or by averaging the parameters of voxels within the ROI. i) Two-tissue compartment model (2TCM): As in the equation for DCE-MRI parameters, $C_a(t)$ is the concentration of $^{13}N$- $NH_3$ in arterial blood and $C_t(t)$ is the concentration of tracer in tissues. This model, which assumes that $^{13}N$ in tissue is in a freely diffusible ($C_e$) (intra- and extravascular) or a metabolically trapped ($C_m$) state, can be expressed as:

$$C_t(t)=C_e(t)+C_m(t)=\frac{K_1}{k_2+k_3}C_a(t)\times[k_3+k_2e^{-(k_2+k_3)t}].$$

Since the rate of diffusion of $^{13}$N- $NH_3$ across the capillary wall is high, the rate constant $K_1$ is an indicator of blood flow. To address the issues of spillover and partial-volume recovery, it was assumed that $C_t(t)=(1-V_a)\cdot C_t(t)+V_a\cdot C_a(t)$ where $C_t(t)$ is the concentration of tracer in tissues; $V_a$ is a real number between 0 and 1; and $(1-V_a)$ is a regional estimate of the tissue partial-volume recovery coefficient. $^{13}$N-$NH_3$ PET perfusion parameters ($K_1$) were estimated using a generalized linear least square method (23). ii) One-tissue compartment model (1TCM): This model assumes that $^{13}$N is present either in blood ($C_a$) or in tissues ($C_t$) and can be expressed as:

$$\frac{dC_t(t)}{dt} = K_1C_a(t) - k_2C_t(t).$$

Using this model, $^{13}$N-$NH_3$ PET perfusion parameters ($K_1$, $k_2$) were estimated using the linear least square method. iii) Voxel-matching of parametric maps from DCE-MRI and $^{13}$N-$NH_3$ PET: The voxel resolutions of DCE-MRI and $^{13}$N-$NH_3$ PET were 1.03×1.03×3 mm and 1.4×1.4×1.4 mm, respectively. For voxel-wise comparison of perfusion parameters between the two methods, parametric map images from PET were re-sliced into the same resolution as those from DCE-MRI using SPM software. Thus, the TACs and input functions at each tumor voxel for both PET and MR images were obtained using the same masking image.

*Statistical analysis*. Pearson's correlation coefficients between MR and PET perfusion parameters were calculated. The adjusted correlation coefficients were calculated in ROI- and voxel-level by the method of Bland and Altman (24, 25) which accounts for the lack of independence among repeated measurements. Correlation coefficients were interpreted as follows; 0-0.3, negligible; 0.3-0.5, low positive; 0.5-0.7, moderate positive; 0.7-0.9, high positive; and 0.9-1.0, very high positive correlation (26). The relationship between MR and PET perfusion parameters on ROI-level was analyzed using a linear/nonlinear regression function. Reproducibility of MR and PET parameters between two successive days on ROI-level were estimated using intra-class correlation coefficients (ICC) by two-way mixed-effects analysis, and ICCs of individual consistency-of-agreement were interpreted as follows; 0-0.2, poor; 0.2-0.4, fair; 0.4-0.6, moderate; 0.6-0.8, good; and 0.8-1.0, excellent correlation. Data analyses were performed using the Stata software package (version 14; Stata, College Station, Tex).

## Results

Of the eight rabbits, one died from air-embolism during the 10-min dynamic MR/PET examination. The remaining seven rabbits successfully underwent MR/PET and were sacrificed after the second MR/PET imaging session by intravenous injection of 5 ml potassium chloride while under deep anesthesia. Unfortunately, because of some error in storage of the raw data of two rabbits, the final analysis included only five rabbits. Representative MR/PET images, arterial input function, and parametric maps are shown in Figures 2 and 3.

*Rabbit tumor characteristics*. VX2 tumors were successfully grown in all five rabbits. The characteristics of rabbit tumors, including tumor size and mean±standard deviation of MR and PET perfusion parameters, are summarized in Table I. The number of ROIs outlining the tumors ranged from 12 to 18 per rabbit (total, 71 ROIs).

*Dynamic $NH_3$ PET modeling*. The AIC, SC, and MSC values of 1TCM and 2TCM are shown in Table II. The 1TCM model was found to be more appropriate model, given its lower AIC and SC values and greater MSC values in comparison to those of the 2TCM model.

*Correlation coefficients between between $K_{trans}$ and $K_1$*. Assuming a linear relationship, there was a positive correlation between MR ($K_{trans}$) and PET ($K_1$) perfusion parameters at the ROI- and voxel-levels (Table III). At the ROI-level, MR and PET perfusion parameters exhibited moderate positive correlations with simultaneous (r=0.54-0.57) and separate (r=0.53-0.69) imaging. At the voxel-level, the two sets of parameters exhibited only negligible correlations with simultaneous (r=0.24) and separate (r=0.16-0.18) imaging.

*Relationship between $K_{trans}$ and $K_1$*. While the $K_{trans}$ and $K_1$ from separate imaging exhibited a linear relationship, those from simultaneous imaging exhibited a nonlinear relationship (Figure 4). The amount of change in $K_1$ associated with a unit increase in $K_{trans}$ varied depending on the values of $K_{trans}$.

*Reproducibility of $K_{trans}$ and $K_1$*. While the ICCs of $K_{trans}$ between simultaneous and separate imaging revealed fair agreement (ICC, 0.29-0.31), those of PET parameters ($K_1$) demonstrated moderate agreement (ICC, 0.44-0.49) (Table IV).

## Discussion

In this study, $K_{trans}$ and $K_1$ exhibited moderate positive correlations with both simultaneous (r=0.54-0.57) and separate (r=0.53-0.69) imaging at the ROI-level, under the assumption of linear relationship between PET and MR parameters, as demonstrated with separate image acquisition. However, careful examination of the association between MR and PET parameters from simultaneous imaging revealed a non-linear relationship between $K_{trans}$ and $K_1$. The amount of change in $K_1$ associated with a unit increase in $K_{trans}$ varied depending on the values of $K_{trans}$.

We believe that a more robust investigation of the relationship between MR and PET perfusion parameters is possible with simultaneous MR/PET than with separate acquisition. Simultaneity is one of the most powerful merits of hybrid MR/PET imaging in comparison with separate PET and MRI or PET/CT, which involves CT followed by PET, hoping that the subject does not move between the two procedures. However, hybrid MR/PET has not been thoroughly investigated, especially in terms of its ability to

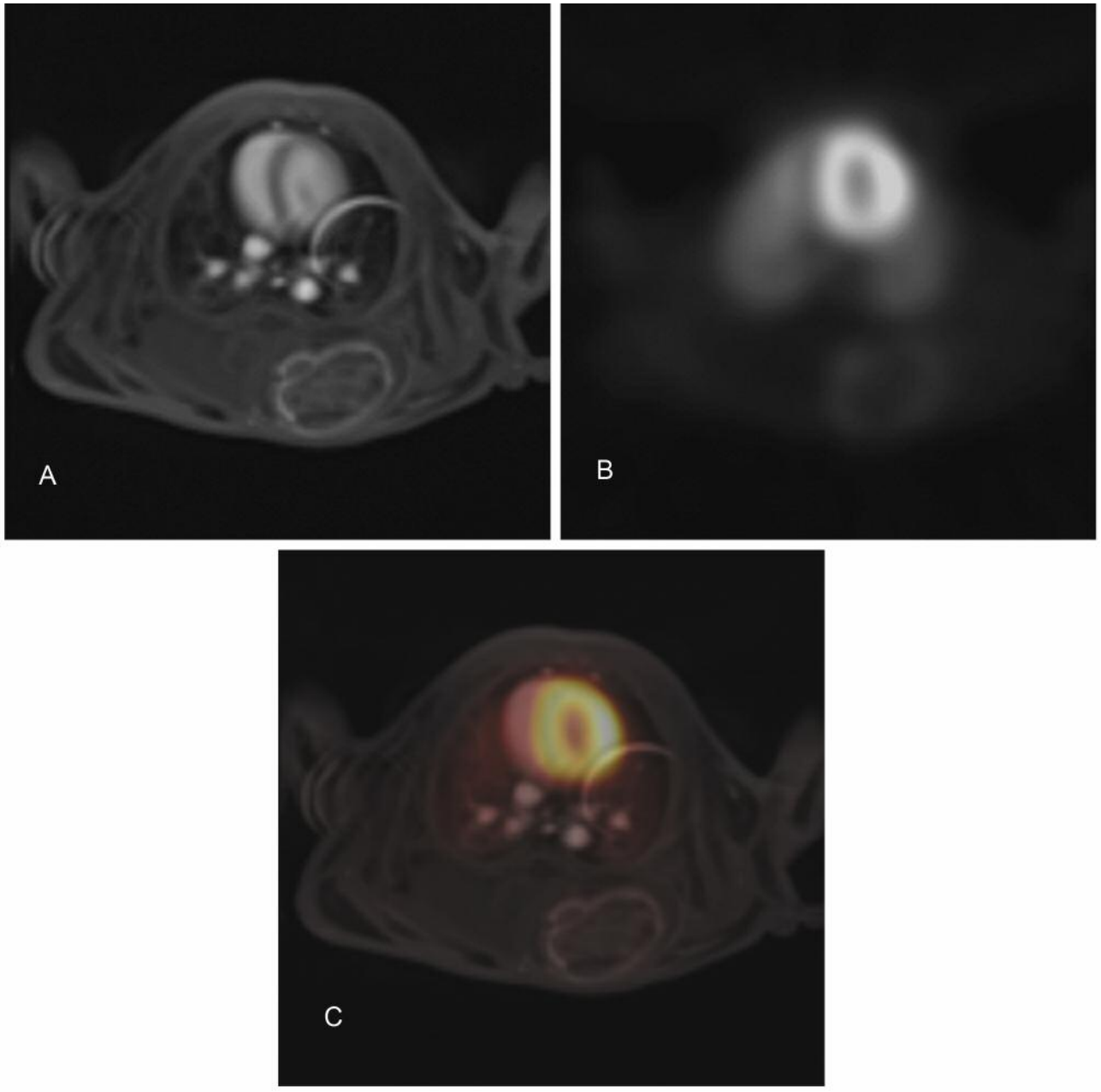


Figure 2. *An example of the MR and PET images. (A) Dynamic contrast-enhanced MR, (B) $^{13}N$-$NH_3$ PET, and C: Fused MR/PET images with simultaneous MR/PET acquisition 14 days after tumor implantation.*

acquire *in vivo* functional information, although its necessity has been recently suggested (14, 27). Simultaneous acquisition not only saves time but also enables better alignment quality (18) and precise evaluation of the relationship between MR and PET parameters under identical tissue microenvironments. Assuming the simple linear correlation between $K_{trans}$ and $K_1$ based solely on separate MR and PET images might result in misinterpretation of the relationship between the two sets of parameters.

Validation of CT and MRI perfusion parameters has been performed mostly in brain and myocardial imaging (28, 29). Unlike perfusion imaging of the myocardium or the brain, there has been no established gold-standard imaging method for tumor perfusion because of the possibility of tissue-

Table I. *Summary of tumor characteristics in five rabbits.*

| Rabbit | | | 1 | 2 | 3 | 4 | 5 |
|---|---|---|---|---|---|---|---|
| Tumor size | Long × short diameter (cm) | | 2.6×2.0 | 2.6×1.8 | 2.6×1.9 | 2.3×2.0 | 2.9×2.6 |
| Simultaneous scan | MR | $K_{trans}$ [$min^{-1}$] | 0.027±0.02 | 0.046±0.04 | 0.038±0.03 | 0.072±0.05 | 0.128±0.14 |
| | | $k_{ep}$ [$min^{-1}$] | 0.142±0.01 | 0.159±0.01 | 0.168±0.02 | 0.228±0.02 | 0.280±0.02 |
| | PET | $K_1$ (1TCM) [mL/min/g] | 0.209±0.11 | 0.301±0.15 | 0.346±0.19 | 0.442±0.19 | 0.389±0.20 |
| | | $k_2$ (1TCM) [$min^{-1}$] | 0.475±0.04 | 0.997±0.10 | 1.147±0.25 | 1.322±0.18 | 1.178±0.22 |
| | | $K_1$ (2TCM) [mL/min/g] | 0.245±0.12 | 0.285±0.13 | 0.367±0.17 | 0.479±0.18 | 0.433±0.20 |
| Separate scan | MR | $K_{trans}$ [$min^{-1}$] | 0.024±0.09 | 0.043±0.06 | 0.033±0.03 | 0.040±0.06 | 0.042±0.04 |
| | | $k_{ep}$ [$min^{-1}$] | 0.045±0.04 | 0.180±0.04 | 0.168±0.03 | 0.308±0.04 | 0.132±0.03 |
| | PET | $K_1$ (1TCM) [mL/min/g] | 0.087±0.05 | 0.157±0.13 | 0.450±0.17 | 0.160±0.09 | 0.287±0.14 |
| | | $k_2$ (1TCM) [$min^{-1}$] | 0.436±0.03 | 0.728±0.14 | 1.467±0.17 | 0.522±0.10 | 0.970±0.15 |
| | | $K_1$ (2TCM) [mL/min/g] | 0.100±0.06 | 0.162±0.13 | 0.433±0.18 | 0.195±0.12 | 0.285±0.14 |

1TCM, 1-tissue compartment model; 2TCM, 2-tissue compartment model. Data are presented as mean±standard deviation.

dependent pathologic vascular abnormalities, such as vascular leakage, shunting, or malformation (30, 31). Instead, validation against histopathological findings such as microvessel density or vascular endothelial growth factors has been attempted for some tumors; however, the results were inconsistent and did not accurately reflect true tumor perfusion *in vivo* (32, 33). Furthermore, pathologic perfusion markers do not reflect perfusion *in vivo*. Therefore, investigation of the relationship between perfusion parameters from two different imaging modalities might serve to cross-validate each parameter. The present results indicate that DCE-MRI perfusion parameters demonstrate a fair amount of blood flow, which is represented by $^{13}$N-$NH_3$ PET perfusion parameters. However, since DCE-MRI perfusion parameters are influenced by both blood flow and permeability, the amount of change in $K_1$ associated with a unit increase in $K_{trans}$ was not always the same. In our study, voxel-level analysis revealed only the negligible correlation between the two parameters. The limited resolution and blurring of PET images might explain this weak correlation on voxel-level and discrepancy between the voxel- and ROI-level analysis.

While $^{13}$N-$NH_3$ PET has been used in myocardial perfusion imaging, only a few studies have examined its utility in tumor imaging (7-10). Prior studies have demonstrated that $^{13}$N-$NH_3$ PET might be a useful imaging tool for semi-quantitative evaluation of tumor perfusion (7-9). Since this is the first study involving quantitative dynamic $^{13}$N-$NH_3$ PET in tumor imaging, we estimated perfusion parameters using two different tissue-compartment models. Although the 2TCM has been widely used in myocardial perfusion, our data indicated that the 1TCM was more appropriate for tumor imaging. This difference might be attributable to the faster circulation time of rabbits and differences in microenvironments and vascular abnormalities within the tumor.

Table II. *Goodness-of-fit parameters of the 1-tissue compartment model (1TCM) and 2-tissue compartment model (2TCM) in $^{13}$N-$NH_3$ PET.*

| | 1TCM | 2TCM |
|---|---|---|
| Simultaneous scan | | |
| AIC | 382.0±10.9 | 400.4±40.4 |
| SC | 386.0±10.9 | 405.6±40.4 |
| MSC | 4.7±0.4 | 4.1±1.5 |
| Separate scan | | |
| AIC | 380.0±33.9 | 397.7±57.6 |
| SC | 384.2±33.9 | 402.9±57.6 |
| MSC | 5.2±1.0 | 4.6±1.5 |

AIC, Akaike information; SC, schwartz; MSC, model selection criteria. Data are presented as mean±standard deviation.

Table III. *Correlation coefficient between MR and PET perfusion parameters with simultaneous scan and separate scan.*

| | Simultaneous scan | Separate scan |
|---|---|---|
| $K_{trans}$ and $K_1$ | | |
| Voxel-level analysis | | |
| 1TCM | 0.24 | 0.18 |
| 2TCM | 0.24 | 0.16 |
| ROI-level analysis | | |
| Average of voxel parameters, 1TCM | 0.55 | 0.65 |
| Average of voxel parameters, 2TCM | 0.57 | 0.58 |
| Single TAC, 1TCM | 0.54 | 0.69 |
| Single TAC, 2TCM | 0.56 | 0.53 |
| $k_{ep}$ and $k_2$ | | |
| ROI-level analysis | | |
| Average of voxel parameters, 1TCM | 0.56 | 0.21 |
| Single TAC, 1TCM | 0.72 | 0.50 |

1TCM, 1-tissue compartment model; 2TCM, 2-tissue compartment model; TAC, time-activity curve.

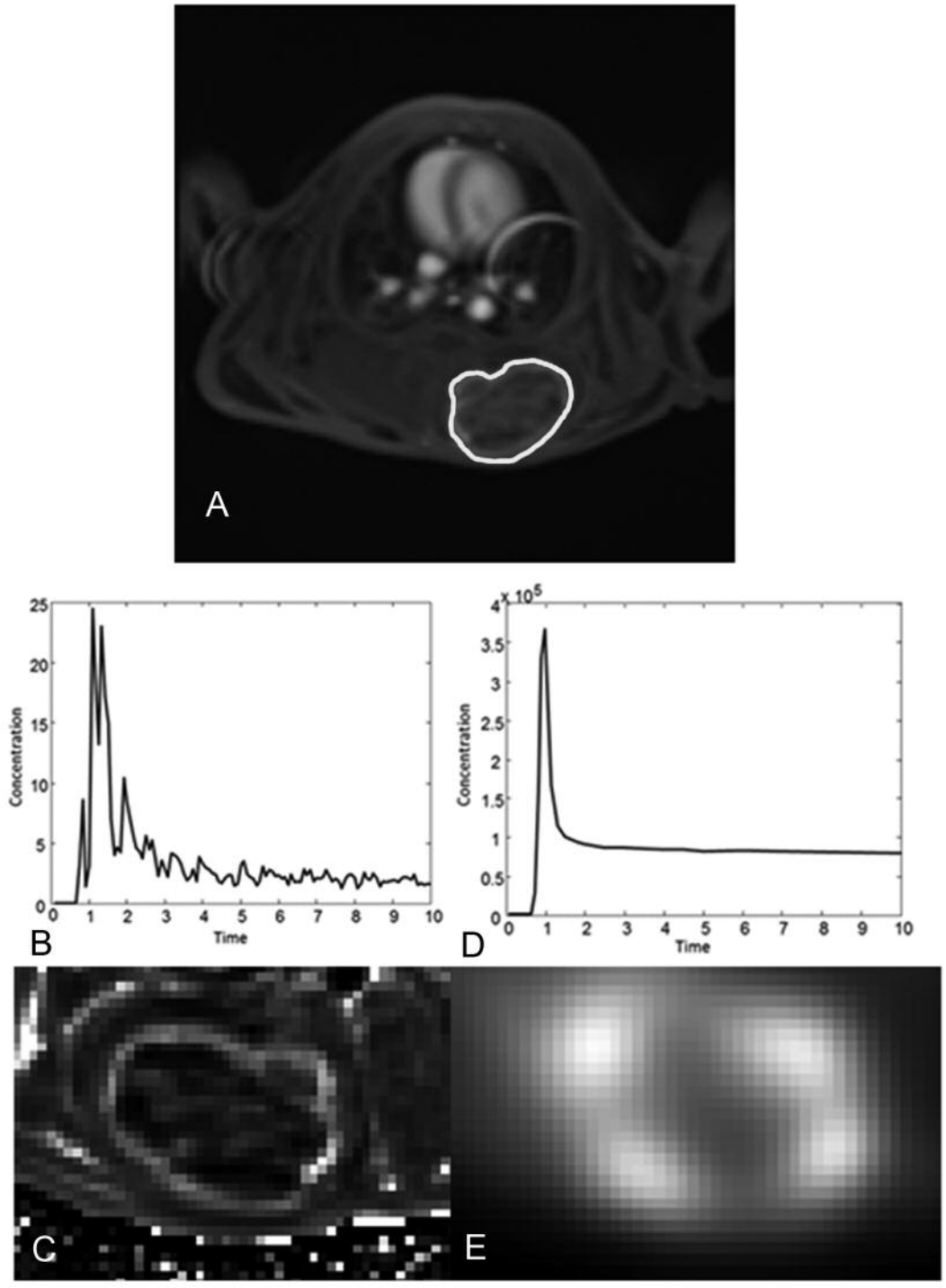


Figure 3. *Parameteric maps of $K_{trans}$ and $K_1$. (A) A representative ROI outlining the entire tumor boundary drawn by a board-certified radiologist on DCE-MRI. (B) Arterial input function curve, and (C) $K_{trans}$ map of DCE-MRI. D: Arterial input function curve, and E: $K_1$ map of dynamic $^{13}N$-$NH_3$ PET using 1-tissue compartment model.*

In the present study, the values of $K_1$ (ICC, 0.44-0.49) were more reproducible than those of $K_{trans}$ (ICC, 0.29-0.31). However, the reproducibilities of $K_1$ and $K_{trans}$ in this study were relatively low when compared to those reported in several previous studies (34-36). Since the reproducibility of perfusion parameters may vary according to the calculation method (37,

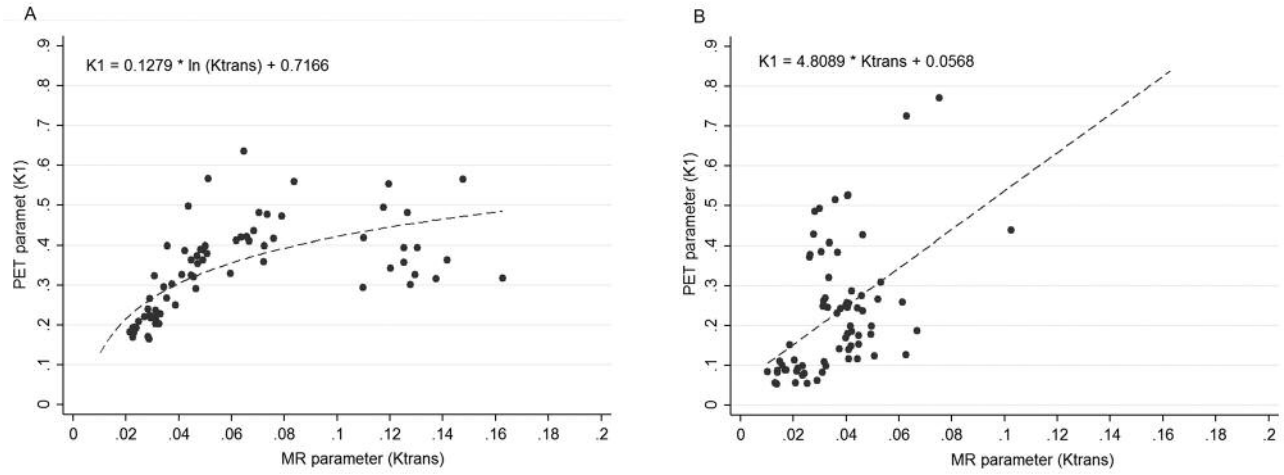


Figure 4. *Scatterplot of ROI values of $K_{trans}$ versus $K_1$. (A) Simultaneous MR/PET acquisition, (B) Separate MR and PET acquisition. In each plot, a dotted line represents an equation estimated with a non-linear and linear regression function, respectively.*

Table IV. *Reproducibility of MR parameters ($K_{trans}$) and PET parameters ($K_1$) on ROI-level between two successive days.*

| | MR parameter ($K_{trans}$) [$min^{-1}$] | PET parameter ($K_1$) [mL/min/g] |
|---|---|---|
| ROI-level analysis | | |
| Average of voxel parameters, 1TCM | 0.29 | 0.46 |
| Average of voxel parameters, 2TCM | 0.29 | 0.49 |
| Single TAC, 1TCM | 0.31 | 0.44 |
| Single TAC, 2TCM | 0.31 | 0.44 |

1TCM, 1-tissue compartment model; 2TCM, 2-tissue compartment model; TAC, time-activity curve.

38), we speculate that the low reproducibility observed in the present study could be due to the one-day gap between simultaneous and separate imaging, calculation of pre-T1 values, estimation of individual AIF or TACs and manual contrast media injection. In addition, in correspondence with the present results, recent studies have demonstrated the low reproducibility of perfusion parameters (39, 40).

There are some limitations to the present study. First, this study included a small number of rabbits. We did not perform additional experiments in order to avoid radiation exposure of the experimenters, although the degree of radiation exposure was relatively low (estimated radiation exposure of the experimenters, 0.0125 mSv per $^{13}N$-$NH_3$ PET examination). Second, we chose $^{13}N$-$NH_3$ as a perfusion marker instead of $^{15}H_2O$, which is regarded as the gold standard for *in vivo* estimation of perfusion in the myocardium and brain, for the following reasons: (a) in comparison $^{15}H_2O$, the longer half-life of $^{13}N$-$NH_3$ (10 min) enables more consistent radiotracer injection among the subjects; (b) the main purpose of this study was to compare simultaneous and separate MR/PET, rather than validation of DCE-MRI, and (c) $^{13}N$-$NH_3$ PET has been under-investigated as a tumor perfusion marker. Finally, since the volume of blood flow and permeability might vary among tumors, the relationship between $K_1$ and $K_{trans}$ might also vary among different tumors.

In conclusion, the relationship between $K_{trans}$ and $K_1$ may be mis-interpreted with separate MR and PET acquisition. Simultaneous MR/PET might allow a more robust investigation of the relationship between MR and PET perfusion parameters than with separate imaging.

## Financial Disclosure

This research was supported by Basic Science Research Program through the National Research Foundation of Korea (NRF) funded by the Ministry of Education (NRF-2013R1A1A2063746), http://nrf.re.kr/. The funder had no role in study design, data collection and analysis, decision to publish, or preparation of the manuscript.

## Acknowledgements

The Authors thank the Medical Research Collaborating Center at Seoul National University Bundang Hospital for statistical analyses.

## References

1 Nielsen T, Wittenborn T and Horsman MR: Dynamic contrast-enhanced magnetic resonance imaging (DCE-MRI) in preclinical studies of antivascular treatments. Pharmaceutics *4(4)*: 563-589, 2012.
2 Padhani AR: Dynamic contrast-enhanced MRI in clinical oncology: current status and future directions. J Magn Reson Imaging *16(4)*: 407-422, 2002.
3 Komori T, Narabayashi I, Matsumura K, Matsuki M, Akagi H, Ogura Y, Aga F and Adachi I: 2-[Fluorine-18]-fluoro-2-deoxy-D-glucose positron emission tomography/computed tomography *versus* whole-body diffusion-weighted MRI for detection of malignant lesions: initial experience. Ann Nucl Med *21(4)*: 209-215, 2007.
4 Cuenod CA, Fournier L, Balvay D and Guinebretiere JM: Tumor angiogenesis: pathophysiology and implications for contrast-enhanced MRI and CT assessment. Abdom Imaging *31(2)*: 188-193, 2006.
5 Schepis T, Gaemperli O, Treyer V, Valenta I, Burger C, Koepfli P, Namdar M, Adachi I, Alkadhi H and Kaufmann PA: Absolute quantification of myocardial blood flow with 13N-ammonia and 3-dimensional PET. J Nucl Med *48(11)*: 1783-1789, 2007.
6 Slomka PJ, Alexanderson E, Jacome R, Jimenez M, Romero E, Meave A, Le Meunier L, Dalhbom M, Berman DS, Germano G and Schelbert H: Comparison of clinical tools for measurements of regional stress and rest myocardial blood flow assessed with 13N-ammonia PET/CT. J Nucl Med *53(2)*: 171-181, 2012.
7 Xiangsong Z and Weian C: Differentiation of recurrent astrocytoma from radiation necrosis: a pilot study with $^{13}N$-$NH_3$ PET. J Neurooncol *82(3)*: 305-311, 2007.
8 Khangembam BC, Karunanithi S, Sharma P, Kc SS, Kumar R, Julka PK, Kumar R and Bal C: Perfusion-metabolism coupling in recurrent gliomas: a prospective validation study with $^{13}N$-ammonia and $^{18}F$-fluorodeoxyglucose PET/CT. Neuroradiology *56(10)*: 893-902, 2014.
9 Xiangsong Z, Changhong L, Weian C and Dong Z: PET Imaging of cerebral astrocytoma with 13N-ammonia. J Neurooncol *78(2)*: 145-151, 2006.
10 Harisankar CN, Mittal BR, Watts A, Bhattacharya A and Sen R: Utility of dynamic perfusion PET using (1)(3)N-ammonia in diagnosis of asymptomatic recurrence of fibrosarcoma. Clin Nucl Med *36(2)*: 150-151, 2011.
11 Eby PR, Partridge SC, White SW, Doot RK, Dunnwald LK, Schubert EK, Kurland BF, Lehman CD and Mankoff DA: Metabolic and vascular features of dynamic contrast-enhanced breast magnetic resonance imaging and (15)O-water positron emission tomography blood flow in breast cancer. Acad Radiol *15(10)*: 1246-1254, 2008.
12 Torigian DA, Zaidi H, Kwee TC, Saboury B, Udupa JK, Cho ZH and Alavi A: PET/MR imaging: technical aspects and potential clinical applications. Radiology *267(1)*: 26-44, 2013.
13 Yoo HJ, Lee JS and Lee JM: Integrated whole body MR/PET: where are we? Korean J Radiol *16(1)*: 32-49, 2015.
14 Yoon SH, Goo JM, Lee SM, Park CM, Seo HJ and Cheon GJ: Positron emission tomography/magnetic resonance imaging evaluation of lung cancer: current status and future prospects. J Thorac Imaging *29(1)*: 4-16, 2014.
15 Chandarana H, Heacock L, Rakheja R, DeMello LR, Bonavita J, Block TK, Geppert C, Babb JS and Friedman KP: Pulmonary nodules in patients with primary malignancy: comparison of hybrid PET/MR and PET/CT imaging. Radiology *268(3)*: 874-881, 2013.
16 Eiber M, Takei T, Souvatzoglou M, Mayerhoefer ME, Furst S, Gaertner FC, Loeffelbein DJ, Rummeny EJ, Ziegler SI, Schwaiger M and Beer AJ: Performance of whole-body integrated $^{18}F$-FDG PET/MR in comparison to PET/CT for evaluation of malignant bone lesions. J Nucl Med *55(2)*: 191-197, 2014.
17 Bailey DL, Antoch G, Bartenstein P, Barthel H, Beer AJ, Bisdas S, Bluemke DA, Boellaard R, Claussen CD, Franzius C, Hacker M, Hricak H, la Fougere C, Guckel B, Nekolla SG, Pichler BJ, Purz S, Quick HH, Sabri O, Sattler B, Schafer J, Schmidt H, van den Hoff J, Voss S, Weber W, Wehrl HF and Beyer T: Combined PET/MR: The Real Work Has Just Started. Summary Report of the Third International Workshop on PET/MR Imaging; February 17-21, 2014, Tubingen, Germany. Mol Imaging Biol *17(3)*: 297-312, 2015.
18 Brendle CB, Schmidt H, Fleischer S, Braeuning UH, Pfannenberg CA and Schwenzer NF: Simultaneously acquired MR/PET images compared with sequential MR/PET and PET/CT: alignment quality. Radiology *268(1)*: 190-199, 2013.
19 Rivera B, Ahrar K, Kangasniemi MM, Hazle JD and Price RE: Canine transmissible venereal tumor: a large-animal transplantable tumor model. Comp Med *55(4)*: 335-343, 2005.
20 Joo I, Lee JM, Grimm R, Han JK and Choi BI: Monitoring vascular disrupting therapy in a rabbit liver tumor model: relationship between tumor perfusion parameters at IVIM diffusion-weighted MR imaging and those at dynamic contrast-enhanced MR imaging. Radiology *278(1)*: 104-113, 2016.
21 Park HS, Han JK, Lee JM, Kim YI, Woo S, Yoon JH, Choi JY and Choi BI: Dynamic contrast-enhanced MRI using a macromolecular MR contrast agent (P792): evaluation of antivascular drug effect in a rabbit VX2 liver tumor model. Korean J Radiol *16(5)*: 1029-1037, 2015.
22 Murase K: Efficient method for calculating kinetic parameters using T1-weighted dynamic contrast-enhanced magnetic resonance imaging. Magn Reson Med *51(4)*: 858-862, 2004.
23 Feng D, Huang SC, Wang ZZ and Ho D: An unbiased parametric imaging algorithm for nonuniformly sampled biomedical system parameter estimation. IEEE Trans Med Imaging *15(4):* 512-518, 1996.
24 Bland JM and Altman DG: Calculating correlation coefficients with repeated observations: Part 1--Correlation within subjects. BMJ *310(6977)*: 446, 1995.
25 Bland JM and Altman DG: Correlation, regression, and repeated data. BMJ *308(6933)*: 896, 1994.
26 Mukaka MM: Statistics corner: A guide to appropriate use of correlation coefficient in medical research. Malawi Med *24(3)*: 69-71, 2012.
27 Bailey DL, Barthel H, Beuthin-Baumann B, Beyer T, Bisdas S, Boellaard R, Czernin J, Drzezga A, Ernemann U, Franzius C, Guckel B, Handgretinger R, Hartenbach M, Hellwig D, Nadel H, Nekolla SG, Pfluger T, Pichler BJ, Quick HH, Sabri O, Sattler B, Schafer J, Schick F, Siegel BA, Schlemmer HP, Schwenzer NF,

van den Hoff J, Veit-Haibach P and Wehrl HF: Combined PET/MR: Where are we now? Summary report of the second international workshop on PET/MR imaging April 8-12, 2013, Tubingen, Germany. Mol Imaging Biol *16(3)*: 295-310, 2014.

28 Raichle ME, Martin WR, Herscovitch P, Mintun MA and Markham J: Brain blood flow measured with intravenous H2(15)O. II. Implementation and validation. J Nucl Med *24(9)*: 790-798, 1983.

29 Bergmann SR, Fox KA, Rand AL, McElvany KD, Welch MJ, Markham J and Sobel BE: Quantification of regional myocardial blood flow *in vivo* with H215O. Circulation *70(4)*: 724-733, 1984.

30 Brix G, Griebel J, Kiessling F and Wenz F: Tracer kinetic modelling of tumour angiogenesis based on dynamic contrast-enhanced CT and MRI measurements. Eur J Nucl Med Mol Imaging *37(Suppl 1)*: S30-51, 2010.

31 Jeswani T and Padhani AR: Imaging tumour angiogenesis. Cancer Imaging *5*: 131-138, 2005.

32 Hulka CA, Edmister WB, Smith BL, Tan L, Sgroi DC, Campbell T, Kopans DB and Weisskoff RM: Dynamic echo-planar imaging of the breast: experience in diagnosing breast carcinoma and correlation with tumor angiogenesis. Radiology *205(3)*: 837-842, 1997.

33 Su MY, Cheung YC, Fruehauf JP, Yu H, Nalcioglu O, Mechetner E, Kyshtoobayeva A, Chen SC, Hsueh S, McLaren CE and Wan YL: Correlation of dynamic contrast enhancement MRI parameters with microvessel density and VEGF for assessment of angiogenesis in breast cancer. J Magn Reson Imaging *18(4)*: 467-477, 2003.

34 Ferrier MC, Sarin H, Fung SH, Schatlo B, Pluta RM, Gupta SN, Choyke PL, Oldfield EH, Thomasson D and Butman JA: Validation of dynamic contrast-enhanced magnetic resonance imaging-derived vascular permeability measurements using quantitative autoradiography in the RG2 rat brain tumor model. Neoplasia *9(7)*: 546-555, 2007.

35 Wang H, Su Z, Ye H, Xu X, Sun Z, Li L, Duan F, Song Y, Lambrou T and Ma L: Reproducibility of dynamic contrast-enhanced MRI in renal cell carcinoma: a prospective analysis on intra- and interobserver and scan-rescan performance of pharmacokinetic parameters. Medicine (Baltimore) *94(37)*: e1529, 2015.

36 Zhang X, Pagel MD, Baker AF and Gillies RJ: Reproducibility of magnetic resonance perfusion imaging. PLoS One *9(2)*: e89797, 2014.

37 Craciunescu O, Brizel D, Cleland E, Yoo D, Muradyan N, Carroll M, Barboriak D and MacFall J: Dynamic contrast enhanced-MRI in head and neck cancer patients: variability of the precontrast longitudinal relaxation time (T10). Med Phys *37(6)*: 2683-2692, 2010.

38 Cron GO, Foottit C, Yankeelov TE, Avruch LI, Schweitzer ME and Cameron I: Arterial input functions determined from MR signal magnitude and phase for quantitative dynamic contrast-enhanced MRI in the human pelvis. Magn Reson Med *66(2)*: 498-504, 2011.

39 Beuzit L, Eliat PA, Brun V, Ferre JC, Gandon Y, Bannier E and Saint-Jalmes H: Dynamic contrast-enhanced MRI: Study of inter-software accuracy and reproducibility using simulated and clinical data. J Magn Reson Imaging *43(6)*: 1288-1300, 2016.

40 Heye T, Davenport MS, Horvath JJ, Feuerlein S, Breault SR, Bashir MR, Merkle EM and Boll DT: Reproducibility of dynamic contrast-enhanced MR imaging. Part I. Perfusion characteristics in the female pelvis by using multiple computer-aided diagnosis perfusion analysis solutions. Radiology *266(3)*: 801-811, 2013.

*Received January 11, 2017*
*Revised February 20, 2017*
*Accepted February 21, 2017*